Experimental and Finite Element Analysis of Flow Behavior of 2A14 Aluminum Alloy during Multi-directional Forging

Ming Wang[1], Juan Wang[2], Wensheng Liu[3], Yunzhu Ma[4], Dongliang Liu[5], Lunwen Guo[6], Lanping Huang[7*], Boyun Huang[8]

[1-8]Science and Technology on High Strength Structural Materials Laboratory, Central South University, Changsha 410083, China

[7]School of Metallurgy and Environment, Central South University, Changsha 410083, China

Abstract— *The deformation flow behavior of 2A14 aluminum alloys during multi-directional forging (MDF) under various cumulative strains ($\sum\Delta\varepsilon$) has been investigated by combining experiment with finite element method (FEM). The forging process has been performed at 450^{o}C with a deformation speed of 0.15 mms^{-1} and a pass strain ($\Delta\varepsilon$) of 0.4. Numerical simulations of MDF using a commercial software (DEFORM-3D), have shown that the vortex, cross-flow and fold defect of flow lines of the forgings do not occur during deformation, and the degree of bent and inhomogeneity of flow lines also increase steadily with $\sum\Delta\varepsilon$ increases. The FEM analysis coincides well with experimental results. The effective strain in various areas of the forgings has been significantly enhanced during MDF. The dynamic recovery is dominant during deformation. The proportion of recrystallized grains and the degree of fragmentation of second phases in various areas of the annealed forgings increase with the increase of effective strain.*

Keywords— 2A14 aluminum alloy, Multi-directional forging, Flow behavior, Effective strain, DEFORM-3D.

I. INTRODUCTION

Severe plastic deformation (SPD), as an effective processing method to fabricate ultrafine or nanostructured metallic materials with excellent properties, has been the subject of intensive investigations over the last two decades [1]. Compared with high-pressure torsion (HPT), equal-channel angular pressing (ECAP) and accumulative roll-bonding (ARB), multi-directional forging (MDF) which involves repeating compression process with changing the axis of the applied strain in three orthogonal directions at each step to obtain fine-grained products and to improve their comprehensive properties, is the simplest and cost-effective method to fabricate bulk products for industrial applications [2-7]. Due to the repeating rotation of the loading direction with deformation passes during MDF, cumulative strain applied from various directions is very significant for the evolution of grain structure and flow behavior of the materials subjected to deformation. A large number of investigations on MDF have indicated that microstructure change during MDF, especially grain refinement, can be controlled by various process factors, such as strain pass, deformation temperature, strain rate, alloying elements, second phase, etc [8-13]. Sitdikov et al. have found that the grain size and its volume fraction in 7475 aluminum alloys during high-temperature multi-directional compression are obviously different from those subjected to uniaxial compression [14]. The reasons are that two deformation modes have different flow behaviors. However, conventional flow analysis only based on experiments is very difficult to use for explaining the deformation behavior very clearly because the flow of metallic materials cannot be observed, so the application of finite element method (FEM) simulation offers convenience to flow analysis of MDF, which makes flow lines behaviors can be seen [15]. Park et al. have predicted metal flows and volume change during die-forging with the rigid-plastic finite element analysis and successfully designed the preform for precision forging of an asymmetric rib-web component [16]. Petrov et al. have applied QFORM-3D for the numerical investigations of the metal flow of isothermal forging and determined the optimum process conditions for isothermal enclosed die forging to fabricate A92618 aluminum alloy part with irregular shape [17]. Otherwise, Zhang et al. investigated the influence of forging process parameters on the distribution of flow lines in 7075 aluminum alloy disk workpiece with complex shape [18]. However, there is almost no work on the flow behaviors of the whole metallic products. Therefore, in this work, the MDF process of 2A14 aluminum alloys has been investigated by finite element software-DEFORM 3D, and the obtained results on the flow behaviors are compared with those obtained by experimental investigations on MDF process.

II. FINITE ELEMENT ANALYSIS

A commercial finite element method (FEM)-code (DEFORM-3D) was used to investigate plastic deformation of 2A14 aluminum alloys during MDF. In the numerical simulations reported here the initial dimension of the billet was 15 mm×12.5 mm×10 mm [14]. The dimensions of the upper and lower anvils of the die were 60 mm in diameter and 20 mm

in length. The FE model of MDF was established by importing three-dimensional images constructed with the CAD software Pro/ENGINEER to DEFORM-3D software. The material of anvils was Inconel 718 alloy. 2014 aluminum alloy was chosen for the forged material. The mesh was generated according to absolute density. The initial mesh with the maximum edge length of 0.3 mm and its size ratio was 1:1, while the final mesh with the minimum edge length of 0.1 mm and its size ratio was 3:1. The isothermal and deformation stages were included in each MDF pass. In the isothermal stages, the initial die temperature and ambient temperature both were 450 ^{o}C, while the initial billet temperature was 25 ^{o}C. Heat transfer coefficient was set to 1 $kWm^{-2}K^{-1}$ and the isothermal time was 8 minutes. In the forging stage, heat transfer coefficient was set to 11$kWm^{-2}K^{-1}$ and the deformation speed 0.15mms^{-1}. A constant friction factor of (m=0.3) was used to define the friction condition at the die-billet interface because this value is often used for hot forging. The forging process ended when the height of the billet was 10 mm. The MDF process was shown in Fig. 1. The initial length (Lx_0), width (Ly_0) and height (Lz_0) of the billet were 12.5 mm, 10 mm and 15 mm, respectively. The pass strain $\Delta\varepsilon$ was all 0.4 and the accumulate strain $\sum\Delta\varepsilon$ was 3.6. In the simulation, the die was considered as a rigid body, while the billet as a rigid-plastic material. The analysis of flow line, effective strain and stress were carried out by the DEFORM-3D software.

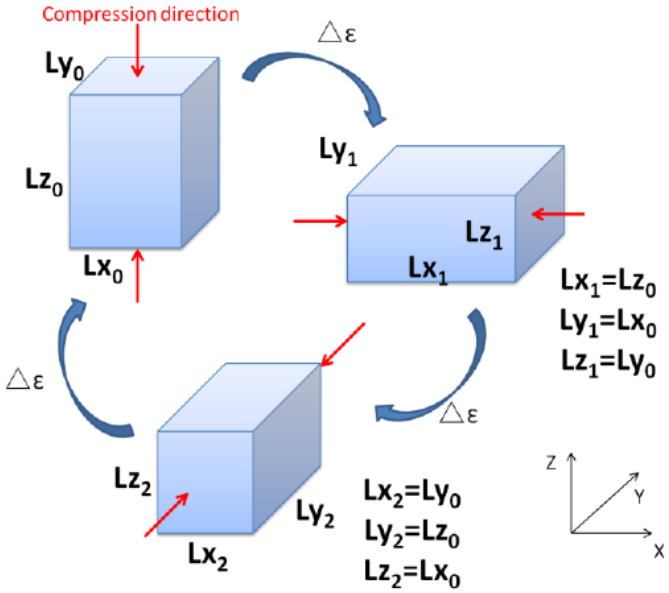

FIGURE. 1: SCHEMATIC ILLUSTRATION OF THE MULTIDIRECTIONAL FORGING (MDF) OF 2A14 ALUMINUM ALLOYS

III. EXPERIMENTAL PROCEDURE

The raw materials used in this work were commercial 2A14 aluminum alloy rods (supplied by Southwest Aluminum (group) Company Ld. China). Its actual chemical composition is 4.76 wt.% Cu, 0.66 wt.% Mg, 0.43 wt.% Si, 0.87 wt.% Mn, 0.20 wt.% Fe and balance Al. The rectangular samples with dimensions of 15 mm×12.5 mm×10 mm were cut from the same part of 2A14 aluminum alloy rods. After being homogenized at 495^{o}C for 12 hours followed by water quenching at room temperature, the samples were alternately forged with loading direction changed through 90°on high-temperature universal testing machine (WSM-200kN) with a deformation speed of 0.15 mms^{-1}. MoS2 was used as high-temperature lubricant between the interface of the anvil and the samples during deformation to alleviate inhomogeneous deformation. After each MDF pass, the sample was quickly quenched, patched and rotated for the next pass. Maximum 9 passes were used. Before MDF, the dies and samples were annealed in an electrical resistance at 450^{o}C for 1 h and 8 minutes, respectively. The material and dimension of the dies were the same as those used for FEM. To observe the recrystallization of the forged samples, the annealing treatment was carried out at 500^{o}C for 1 h. The T6 aging treatment was conducted by holding the annealed samples at 160°C for 12 h followed by air cooling for the micro-hardness measurement.

The central cross-sections of the samples parallel to the last loading axis were used for FEM and microstructural analysis. The schematic illustration was shown in Fig.2. Microstructural analysis was performed by optical microscopy (OM, Leica DFC 500) and scanning electron microscopy (SEM, FEI Nova Nano 230). The polished samples prepared for the low- and high-magnified OM were etched in 50% NaOH solution and Kerr agent containing 5 ml HNO_3, 2 ml HF, 3 ml HCl and 190 ml water, respectively. The micro-hardness measurement was performed using a typical Vickers hardness tester with an

applied load of 1 kg for a dwell time of 15 s and 8 spots for each sample were selected, and then average value and standard deviation were calculated.

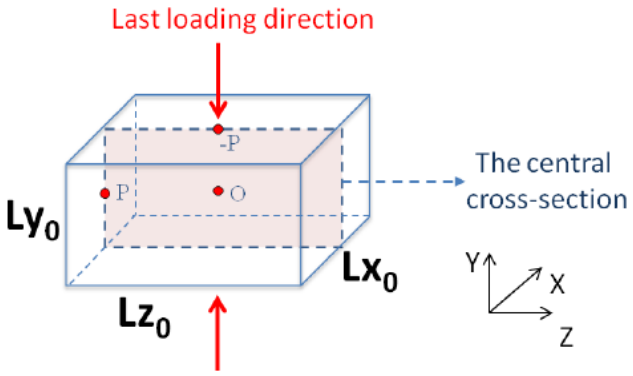

FIGURE. 2 VIEWING PLANE OF 2A14 ALUMINUM ALLOYS PROCESSED BY MDF AND ANALYTICAL PLANE OF FEM

IV. RESULTS AND DISCUSSION

4.1 Forging process

The FEM-simulated and experimental stress–strain curves of 2A14 aluminum alloys during the first MDF pass are shown in Figure 3. It can be seen that the two flow stress-strain curves are remarkably similar and both exhibit sharp stress peak just after yielding, followed by work softening. The experimental curve shows a steady stress with a significant decrease after $\Delta\varepsilon$ beyond 0.1. In contrast, the FEM-simulated curve presents a steady-state-like flow behavior. The difference of the flow stresses between FEM and experiments was mainly attributed to the constitutive equation used for 2A14 aluminum alloy in this work neglecting the softening of materials. Nevertheless, the subtle difference has little impact on the simulation results of flow line and effective strain distribution during MDF process.

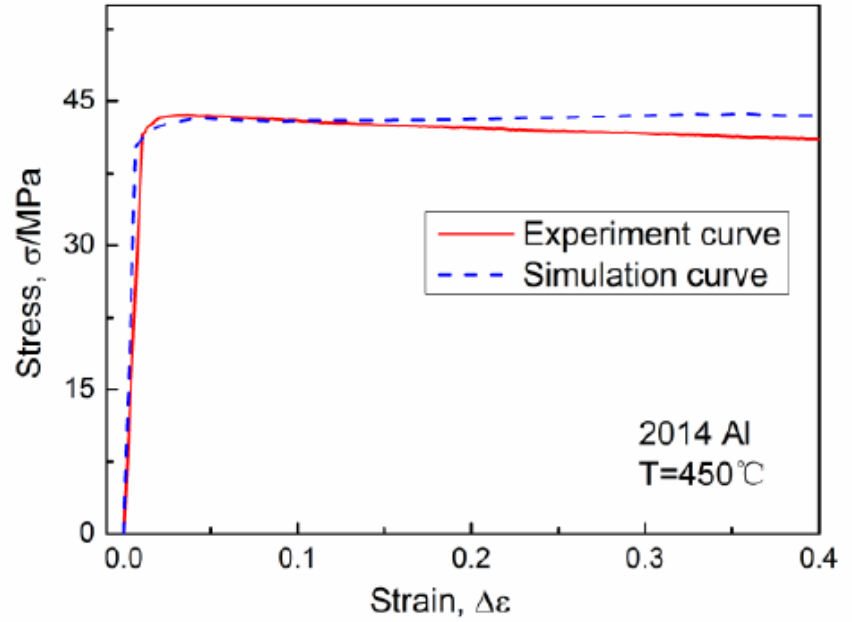

FIGURE 3 FEM-SIMULATED AND EXPERIMENTAL STRESS–STRAIN CURVES DURING THE FIRST MDF PASS OF 2014 ALUMINUM ALLOYS AT 450^{o}C AND AT A DEFORMATION SPEED OF 0.15 mms^{-1}

Figure 4 presents the appearances of the billets during MDF obtained by experiments and FEM. The experimental results show that the shapes of samples before and after MDF remain unchanged basically. However, there are some bulges in x direction and z direction, which are caused by the friction between billets and anvils. With the increase of forging passes, the bulges have a trend to become more obvious. The FEM analysis coincides well with experimental results, which indicates that the selected parameters used for the FEM analysis are suitable for the simulation of MDF process of 2A14 aluminum alloy.

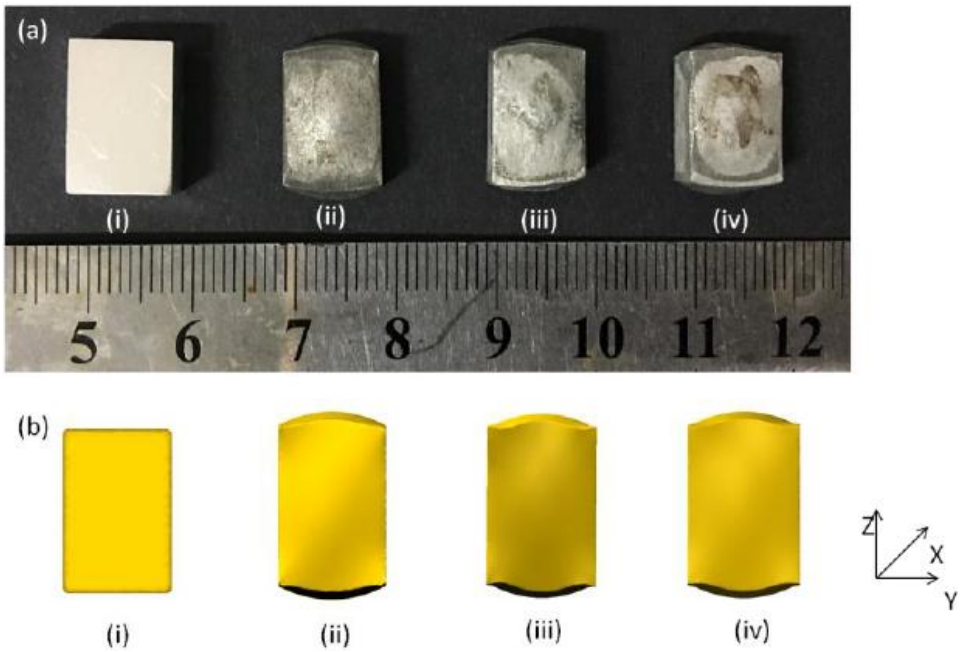

FIGURE 4 APPEARANCES OF THE 2A14 ALUMINUM ALLOY BILLETS DURING MDF OBTAINED BY (a) EXPERIMENTS AND (b) FEM: (i) BEFORE MDF; (ii) ∑Δ ε=1.2; (iii) ∑Δ ε=2.4; (iv) ∑Δ ε=3.6

4.2 Effects of cumulative strain on flow lines

To keep tracking of the materials flow during MDF, a flow-net technique was used in the FEM simulation. The flow lines distribution of the cross section of 2A14 aluminum alloys under various cumulative strain during MDF are shown in Figure 5. In Figure 5(a), the size of mesh was 0.42×0.42 mm, which was generated by setting the initial lateral and vertical flow lines. With the increase of cumulative strain, the vortex and outcrop defects did not exist, but flow lines in some areas were obviously bended, which led to the formation of considerable distorted meshes. When ∑Δ ε=0.4 (shown in Fig.5(b)), the billet was only subjected to compressed deformation in the axial direction, so the vertical flow lines were slightly bended toward the outer edge, and the lateral flow lines were bended toward the corners nearby. The meshes were stretched and the deformation extent in the center was relatively large, while the deformation extent on the surface between the die and billet were slightly small. The mesh deformation in various areas was obviously inhomogeneous. This inhomogeneity was attributed to non-uniform MDF deformation. The difference of deformation degrees during forging resulted into the formation of four deformation zones in the deformed billet, namely easy deformation zone I, shear deformation zone II, free deformation zone III and hard deformation zone IV, as shown in Fig. 5(c). The zone I and II showed an X-shape and were in the center of the sample, where high plastic deformation could be easily obtained. The zone III was close to the free end surfaces and exhibited two hemispheric shapes. During forging, the capacity of plastic deformation in this zone was between the easy deformation zone and hard deformation zone. The zone IV was close to the two anvils and its shape was similar to that of zone III. In this zone, the friction between the anvils and the sample impeded the flow of the metal leading to the hard-plastic deformation.

According to the distribution patterns of flow lines of the MDF samples, the meshes in the cross section could also be divided into the four deformation zones, as indicated in Fig. 5(b), (d), (e) and (f). When ∑Δ ε>0.4 (shown in Fig. 5(d)-(f)), the billet was subjected to multidirectional deformation, compared with uniaxial deformation, the characteristics of flow lines in this four zones were more apparent. In zone I, the meshes were square and its size slightly decreased compared with the initial ones, which were different from the tensile meshes normal to compression direction during uniaxial compression. The meshes in zone II were diamond and the bend degree of flow lines increased with cumulative strain increased. The meshes in zone III were also square, which were similar to those in zone I, and the mesh size slightly increased with cumulative strain increased. When ∑Δ ε=3.6 (shown in Fig. 3(d)), the mesh size was equal to that of the initial mesh. In zone IV the meshes were stretched along compression direction and mesh density also increased with cumulative strain increased. Compared with the free forging process, MDF changed flow lines distribution in zone IV and enhanced the degree of deformation. Therefore, the inhomogeneous degree of the formed meshes gradually increased with the evolution of flow lines during MDF.

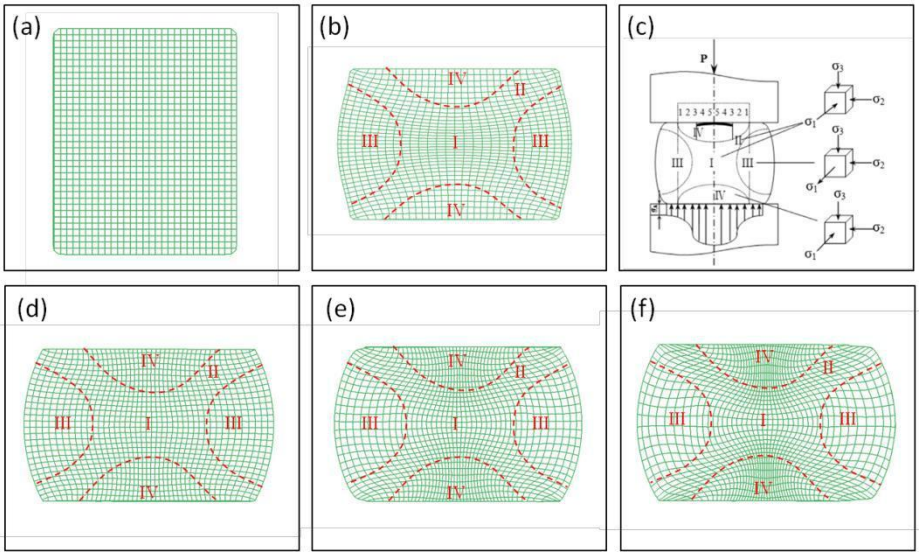

FIGURE 5: CROSS SECTIONS OF THE SIMULATED FLOW LINES OF 2A14 ALUMINUM ALLOYS PROCESSED BY MDF UNDER VARIOUS CUMULATIVE STRAINS: (a) ΣΔε=0; (b) ΣΔε=0.4; (c) SCHEMATIC DIAGRAM OF FOUR DEFORMATION ZONES DURING MDF; (d) ΣΔε=1.2; (e) ΣΔε=2.4 (f) ΣΔε=3.6

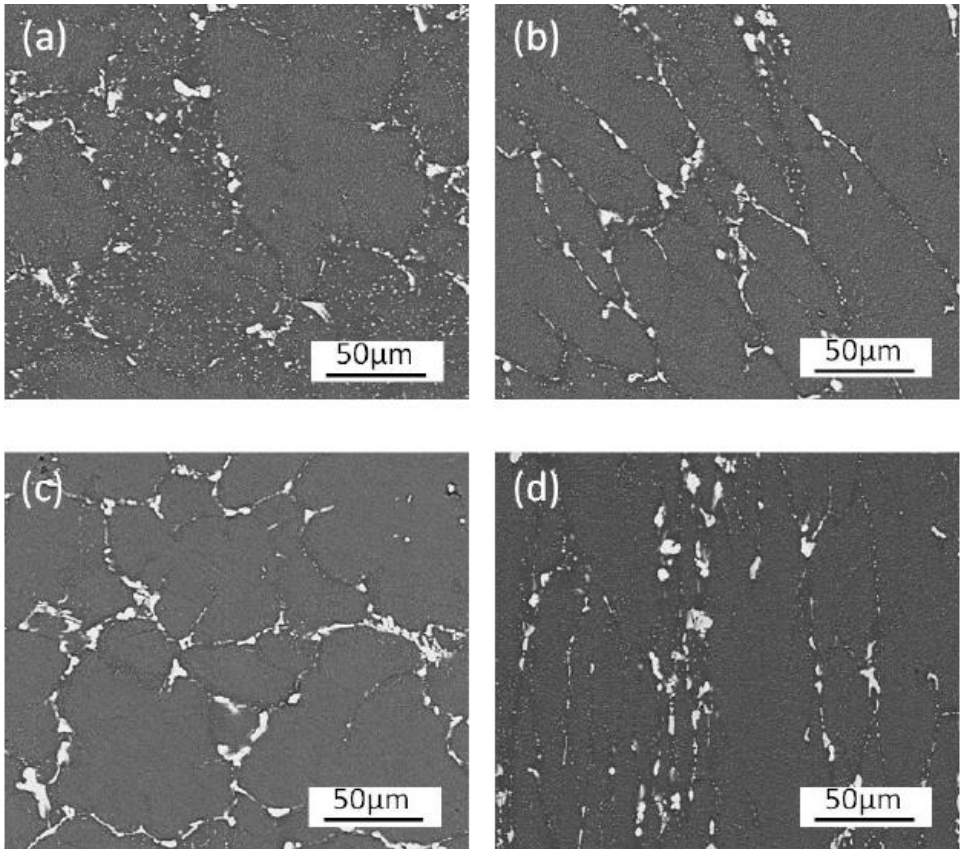

FIGURE 6: SEM IMAGES OF 2A14 ALUMINUM ALLOYS PROCESSED BY MDF IN DIFFERENT ZONES WITH ΣΔε=3.6: (a) Zone I; (b) Zone II; (c) Zone III; (d) Zone IV

Figure 6 presents the SEM images of the 2A14 aluminum alloy obtained by MDF. As shown in Fig. 6, the intensity and orientation distribution of flow lines of the 2A14 aluminum alloy forgings coincided well with the simulated results. The high magnified SEM images were described as follow: the grains in zone I (shown in Fig. 6(a)) were repeatedly tensioned and compressed, so the second phase particles were completely broken. Besides, a great number of second phase particles existed in grain interiors. In zone II flow lines were bent and the direction along which the grains were stretched was at a 45° to compression direction. The grains in zone III were near isometric, which corresponds to the almost unchanged meshes in

this zone during MDF process. On the contrary, the grains in zone IV were stretched along compression direction and their distortion degree was large. During MDF process, the position of zone III and zone IV were exchanged, so there were some broken second phase particles along grain boundaries in hard-plastic deformation zone IV. Since the flow lines of aluminum alloy forgings have obvious effects on their mechanical properties, the control of flow lines is always one of the key in the production of forgings [18]. The accurate prediction for flow lines during MDF provides a convenient and effective way for the control of flow lines in the practical forging process.

4.3 Effects of cumulative strain on effective strain

Figure 7 shows the effective strain distribution of the deformed 2A14 aluminum alloy workpieces with various cumulative strains during MDF. It can be seen that the distribution of the effective strain is inhomogeneous in the workpieces and the values of the effective strain gradually increase with the increase of cumulative strain. Large deformation occurs in the center and corners of the workpiece, while the plastic deformation is very difficult at the regions between the workpiece and the die due to high friction. In addition, it can be also seen from the strain values that the strain level in the larger cumulative strain is the higher. Overall, the values of effective strain gradually decrease from the center (point O in Fig. 2) toward the contact surface (point P in Fig. 2) and the edge (point –P in Fig. 2). The quantitative comparison of the effective strain from point –P to point O, then to point P of the deformed workpieces with various cumulative strains is shown in Fig. 8. It can be found that the minimum value of the effective strain is 0.428, and its maximum value in the center with large deformation is 0.843 when $\sum\Delta\varepsilon=0.4$. The effective strain in various regions continuously accumulates with increasing the total cumulative strain. When $\sum\Delta\varepsilon=3.6$, the minimum value of the effective strain is 1.94, and its maximum value in the center is up to 6.9. This means that the MDF process can obviously enhance the effective strain in various regions, and thus improve the microstructure and properties of the 2A14 aluminum alloys. Meanwhile, when the workpiece is subjected to uniaxial compression ($\sum\Delta\varepsilon=0.4$), the minimum value of the effective strain is distributed at the contact surface of the workpiece (point P), when subjected to MDF ($\sum\Delta\varepsilon>0.4$), its minimum value is alternately distributed at the contact surface (point P) and the edge (point –P). Therefore, the distribution of the effective strain during MDF exhibits different characteristics compared with uniaxial compression. It is favorable for improving the deformation characteristic of hard deformation zone at the contact area between the workpiece and the die by steadily changing the compression direction during forging.

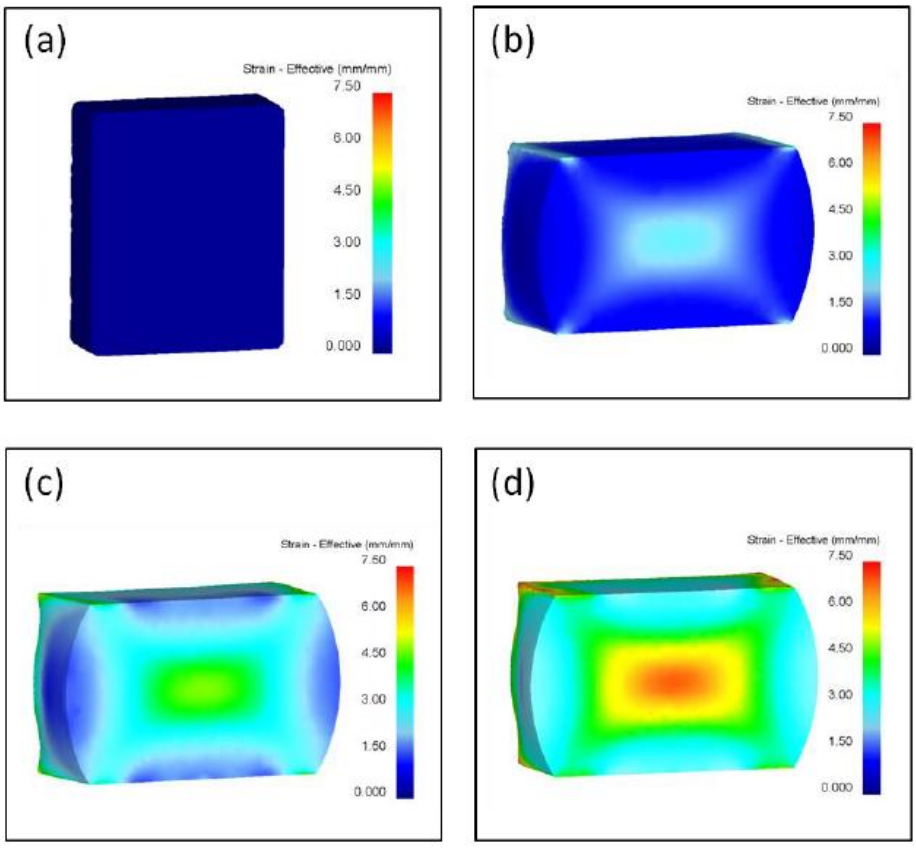

FIGURE 7 DISTRIBUTION OF EFFECTIVE STRAIN IN CROSS SECTION OF 2A14 ALUMINUM ALLOYS PROCESSED BY MDF WITH VARIOUS CUMULATIVE STRAINS: (a) $\Sigma\Delta\varepsilon=0$; (b) $\Sigma\Delta\varepsilon=1.2$; (c) $\Sigma\Delta\varepsilon=2.4$; (d) $\Sigma\Delta\varepsilon=3.6$

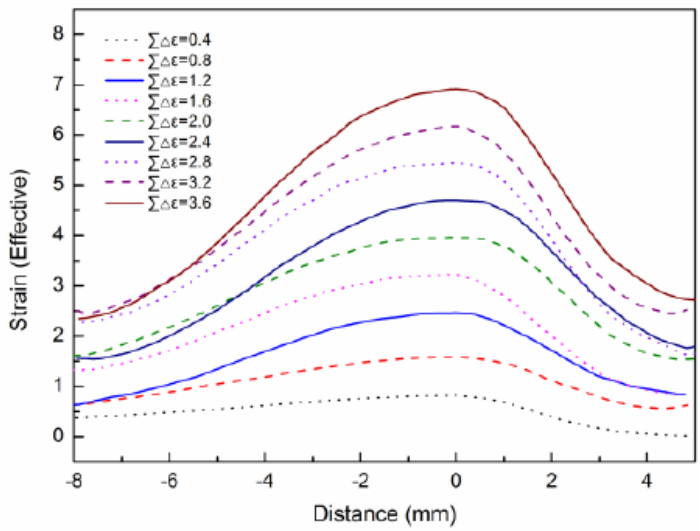

FIGURE 8: RELATIONSHIP BETWEEN EFFECTIVE STRAIN AND THE DISTANCE FROM THE EDGE OF THE DRUM SHAPE (POINT –P) TO THE CENTER (POINT O), THEN TO THE CONTACT SURFACE (POINT P)

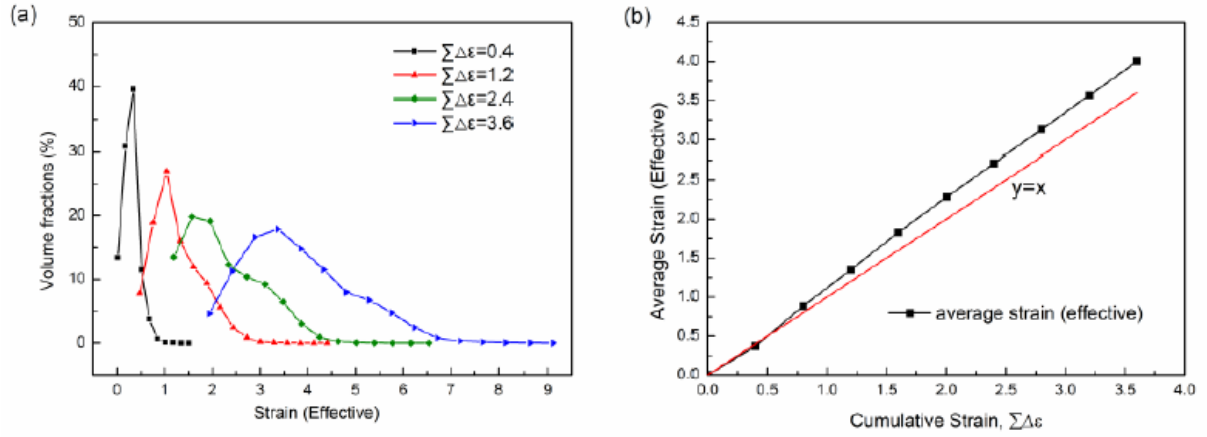

FIGURE 9: (a) EVOLUTION OF THE VOLUME FRACTION OF EFFECTIVE STRAIN WITH AVERAGE EFFECTIVE STRAIN; (b) EVOLUTION OF AVERAGE EFFECTIVE STRAIN WITH CUMULATIVE STRAIN

To further investigate the distribution of the effective strain during MDF, the analysis of the volume fraction of the effective strain and average effective strain are also carried out. Figure 9(a) shows the relationship between the volume fractions of the effective strain and cumulative strain of 2A14 aluminum alloy during MDF. With cumulative strain increases the effective strain in various areas are all enhanced but its heterogeneity also gradually increases. It can be also seen in Fig. 9(b) that the distribution range of the effective strain also becomes wider and the average effective strain is also higher. When $\sum\Delta\varepsilon>0.6$, the average effective strain is higher than the total cumulative strain and the difference between them becomes larger. This means that the steadily increase of cumulative strains can enhance the mobility of metals in hard deformation region. Therefore, it is a feasible way for enhancing the properties of the forgings by steadily increasing cumulative strain during MDF, but how to improve its homogeneity needs to be further studied in the future.

4.4 Effects of cumulative strain on recrystallization microstructure

Figure 10 shows the optical microstructures of zone I, II, III and IV of the deformed and annealed forgings. When $\sum\Delta\varepsilon=3.6$, it can be seen from Fig. 10(a) that the microstructure exhibits the characteristic of dynamic recovery and the deformed microstructures at different regions are obviously different. The size and appearance of grains coincide well with the simulation results of flow lines. As above mentioned, the value of effective strain in these four zones are ranged as follows: I>II>IV≈III. This shows that the degree of fragmentation of second phase particles gradually increases with the increase of effective strain. To further investigate the recrystallization of 2A14 aluminum alloy forgings, the optical microstructures of the annealing samples are shown in Fig. 10(b). It can be found that partial recrystallized grains exist on the boundary of the initial grains, and the recrystallization in various regions is also different. The size of recrystallized grains gradually decreases with the increase of cumulative strain, while volume fraction increases. The difference of effective strain in various

regions is mainly responsible for the inhomogeneity of recrystallization. It is generally believed that dynamic recrystallization does not occur in aluminum alloys due to its high fault energy, but recently some work have shown that the distinct dynamic recrystallization microstructure can be found during the compression deformation of some Al-Zn-Mg-Cu and Al-Cu-Mg-Ag aluminum alloy systems [19-22]. In 2A14 aluminum alloys the dislocation easily moves and cross slips, so the steady sub-microstructure can be formed during deformation process, and thus continuous dynamic recrystallization only occurs in the range of sub-grains [23]. Dynamic recovery has a predominant role in the MDF of 2A14 aluminum alloys, while dynamic recrystallization is difficult to proceed completely. After annealing treatment, the energy stored in sub-grain nearby is released, so continuous dynamic recrystallization takes place and recrystallized grains completely grow up. The different of effective strain results in the difference of the accumulation and the degree of entanglement of the dislocation in various regions, and thus leads to the difference of the recrystallization nucleation rate. Therefore, the fraction of recrystallization is also non-uniformly distributed.

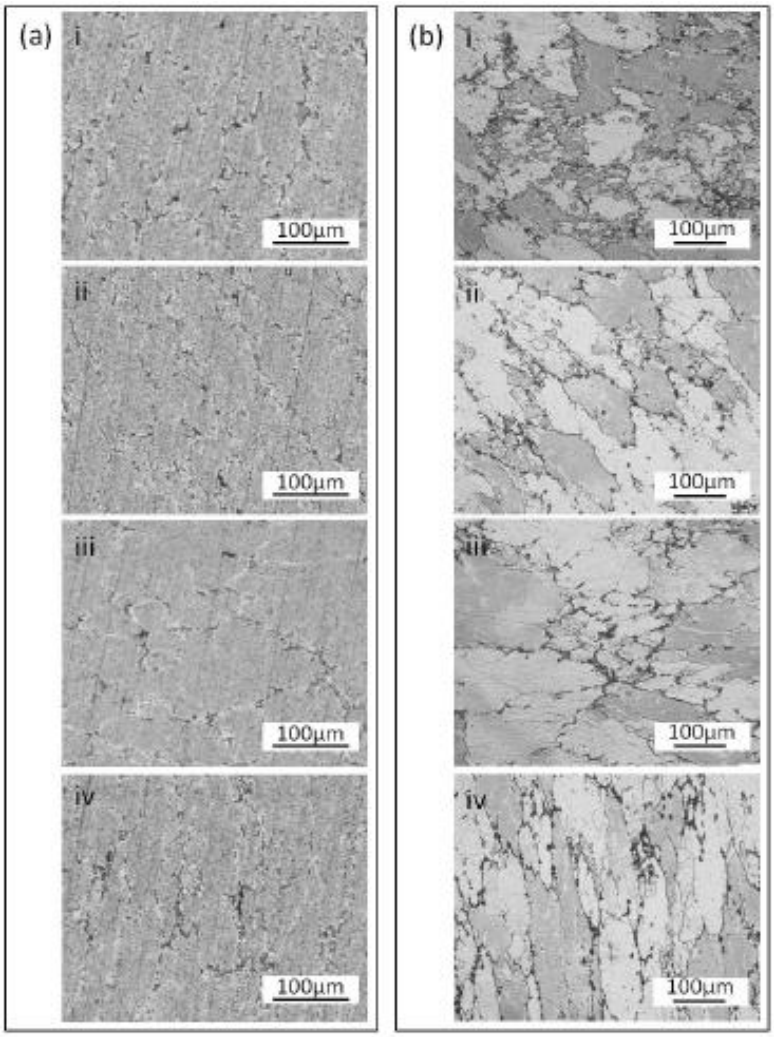

FIGURE 10: OPTICAL MICROSTRUCTURES OF THE DEFORMED (a) and annealed (b) 2A14 aluminum alloys obtained by MDF in different zones with ∑Δε=3.6: (i) Zone I; (ii) Zone II; (iii) Zone III; (iv) Zone IV

The inhomogeneity of the strain increases with the increase of ∑Δε in the forging process, but its homogeneous degree can be improved with the increase of ∑Δε. In order to evaluate the relationship between mechanical property and strain during MDF process, the Vickers hardness in various zones of the center interface of this alloy was measured. As shown in figure 11, the microhardness values in various zones are slightly different due to the difference of deformation degree. The microhardness values are ranged as followed: I>II>IV≈III, which coincide well with the simulation results of effective strains. This suggests that the distribution of equivalent strain simulated by FEM can predict the changing trends of the hardness. Meanwhile, the difference of the microhardness in various zones gradually decreases with the increase of cumulative strain. This means that the inhomogeneity of deformation of 2A14 aluminum alloy during forging can be improved by increasing ∑Δε.

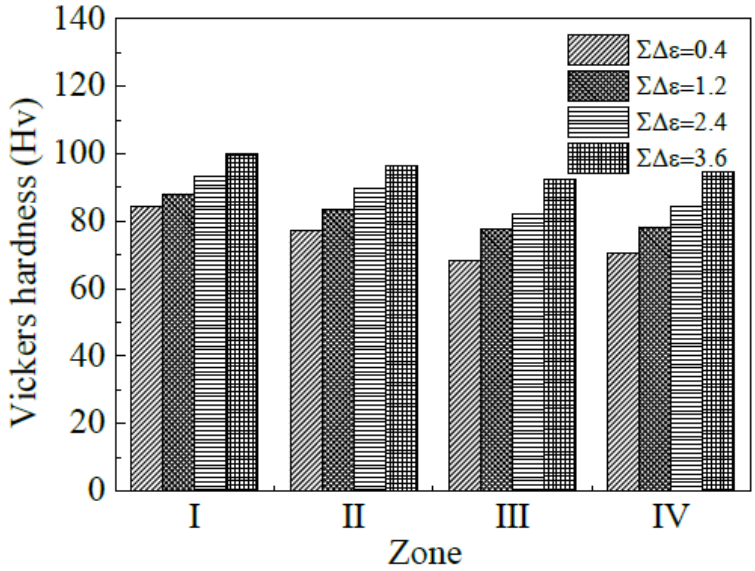

FIGURE 11: DISTRIBUTION OF VICKERS HARDNESS IN FOUR DEFORMATION ZONES FOR 2A14 ALUMINUM ALLOYS WITH DIFFERENT NUMBERS OF MDF PASSES

V. CONCLUSION

In this work, the deformation flow behavior of 2A14 aluminum alloy processed by MDF has been investigated by combining experiment with finite element method (FEM). Experiments were carried out to validate the simulated results. The results are summarized as follow:

(1) The evolution with respect to the metal flow in 2A14 aluminum alloy forgings during MDF can be accurately simulated by FEM. With cumulative strain increases the heterogeneity of flow lines is obviously enhanced. The meshes in some areas are steadily stretched and flow lines are significantly bent.

(2) The effective strain in various areas of 2A14 forgings is steadily accumulated with the increase of cumulative strain.

When cumulative strain $\sum\Delta\varepsilon=3.6$, the minimum value of effective strain is 1.94, and its maximum value is up to 6.9 in the center with high deformation degree. It is favorable for the improvement of deformation capacity of hard deformation area by MDF.

(3) The degree of fragmentation of grains and second phases on the grain boundary is obviously enhanced with the steady accumulation of effective strain in various areas of 2A14 forgings. It can be effectively predicted that the refinement degree of grains and second-phase particles in various areas by using FEM to simulate the evolution of effective strain of the forgings.

(4) The dynamic recovery microstructure can be found in the 2A14 aluminum alloy forgings processed by MDF. After annealing treatment, the size of recrystallized grains gradually decreases while its volume fraction steadily increases with the increase of effective strain.

ACKNOWLEDGEMENTS

This work was primarily financial supported by the National Natural Science Foundation of China (Grant No. 51201186) and National High-technology Research and Development Program of China (863 Program) (Grant No. 2009AA034300) as well as State Key Laboratory for Powder Metallurgy and Science and Technology on High Strength Structural Materials Laboratory, Central South University.

REFERENCES

[1] R. Z. Valiez, R. K. Islamgaliev and I. V. Alexandrov, "Bulk nanostructured materials from severe plastic deformation," Prog Mater Sci. vol.45 (2), pp. 103-189, 2000.

[2] R. Yoda, K. Shibata, T. Morimitsu, D. Terada and N. Tsuji, "Formability of ultrafine-grained interstitial-free steel fabricated by accumulative roll-bonding and subsequent annealing," Scripta Mater. vol.65, pp. 175-178, 2011.

[3] A. A. Mazilkin, B. B. Straumal, M. V. Borodachenkova, R. Z. Valiev, O. A. Kogtenkova and B. Baretzky, "Gradual softening of Al-Zn alloys during high-pressure torsion," Mater Lett. vol.84, pp. 63-65, 2012.

[4] M. Zha, Y. Li, R. H. Mathiesen, R. Bjørge and H. J. Roven, "Microstructure evolution and mechanical behavior of a binary Al-7Mg alloy processed by equal-channel angular pressing," Acta Mater. vol.84, pp. 42–54, 2015.

[5] K. B. Nie, K. K. Deng, X. J. Wang, F. J. Xu, K. Wu, M. Y. Zheng, "Multidirectional forging of AZ91 magnesium alloy and its effects on microstructures and mechanical properties," Mater Sci Eng A. vol.624, pp. 157-168, 2015.

[6] M. R. Jandaghi, H. Pouraliakbar, M. Khanzadeh, G. Khalaj and M. Shirazi, "On the effect of non-isothermal annealing and multi-directional forging on the microstructural evolutions and correlated mechanical and electrical characteristics of hot-deformed Al-Mg alloy," Mater Sci Eng A. vol.657, pp. 431-440, 2016.

[7] D. Desrayaud, S. Ringeval and S. Girard, "A novel high straining process for bulk materials-The development of a multi-Pass forging system by compression along three axes," J Mater Process Technol. vol.172(1), pp. 152-158 , 2006.

[8] A. Danno, C. C. Wong, S. Tong, A. Jarfors, K. Nishino and T. Furuta, "Effect of cold severe deformation by multi directional forging on elastic modulus of multi functional Ti + 25 mol% (Ta, Nb, V) + (Zr, Hr, O) alloy," Mater Des. vol.31(6), pp. 61–65, 2010.

[9] H. Miura, G. Yu, X. Yang and T. Sakai, "Microstructure and mechanical properties of AZ61 Mg alloy prepared by multi directional forging," Trans Nonferrous Met Soc China. vol.20(7), pp. 1294-1298, 2010.

[10] H. Miura, T. Maruoka, X. Yang and J. J. Jonas, "Microstructure and mechanical properties of multi-directionally forged Mg–Al–Zn alloy," Scripta Mater. vol.66(1), pp. 49-51, 2012.

[11] O. Sitdikov, T. Sakai, H. Miura and H. Hama, "Temperature effect on fine-grained structure formation in high-strength Al alloy 7475 during hot severe deformation," Mater Sci Eng A. vol.516(1-2), pp. 180-188, 2009.

[12] O. Sitdikov, T. Sakai, A. Goloborodko and R. Kaibyshev, "Effect of pass strain on grain refinement in 7475 Al alloy during hot multidirectional forging," Mater Trans. vol.45(7), pp. 2232-2238, 2004.

[13] A. Belyakov, K. Tsuzaki, H. Miura and T. Sakai, "Effect of initial microstructures on grain refinement in a stainless steel by large strain deformation,"Acta Mater. vol.51(3), pp. 847-861, 2003.

[14] O. Sitdikov, T. Sakai, A. Goloborodko and H. Miura, "Grain fragmentation in a coarse-grained 7475 Al alloy during hot deformation," Scripta Mater. vol.51(2), pp. 175-179, 2004.

[15] A. N. Bramley and D. J. Mynors, "The use of forging simulation tools," Mater Des. vol.21(4), pp. 279-286, 2000.

[16] J. J. Park and H. S. Hwang, "Preform design for precision forging of an asymmetric rib-web type component," J Mater Process Technol. vol.187–188, pp. 595–599, 2007.

[17] P. Petrov, V. Perfilov and S. Stebunov, "Prevention of lap formation in near net shape isothermal forging technology of part of irregular shape made of aluminium alloy A92618," J Mater Process Technol. vol.177(1-3), pp. 218–223, 2006.

[18] Y. Q. Zhang, D. B. Shan and F. C. Xu, "Flow lines control of disk structure with complex shape in isothermal precision forging," J Mater Process Technol. vol.209(2), pp. 745-753, 2009.

[19] J. Zhou, T. J. Zhang, X. M. Zhang, G. L. Ma, F. Tian and L. Zhou, "The influence of forge mode on dynamic recrystallization for 7075 aluminum alloy during forging," Rare Metal Mater Eng. vol.33(8), pp. 827-830, (2004.

[20] T. Sakai, H. Miura, A. Goloborodko and O. Sitdikov, "Continuous dynamic recrystallization during the transient severe deformation of aluminum alloy 7475," Acta Mater. vol.57(1), pp. 153-162, 2009.

[21] S. Yang, D. Q. Yi, H. Zhang and S. J. Yao, "Flow stress behavior and processing map of Al-Cu-Mg-Ag alloy during hot compression," J Wuhan Univ Technol Mater Sci Ed. vol.23(5), pp. 694-698, 2008.

[22] X. Y. Liu, Q. L. Pan, Y. B. He, W. B. Li, W. J. Liang and Z. M. Yin, "Flow stress behavior and microstructure of Al-Cu-Mg-Ag alloy during hot compression deformation," Chin J Nonferrous Met. vol.19(2), pp. 201-207, 2009.

[23] J. P. Lin, X. Y. An and T. Q. Lei, "A dynamic recrystallization model of Al-alloys," J Univ Sci Technol Beijing. vol.15(30), pp. 262-266, 1993.